A Soft Durometer for Tactile Sensing

Marcos Oliveira[1], Akshay Vaidya[1], Taskin Padir[2], and Samuel Felton[1]

***Abstract*— The food industry is dependent on human labor for tasks that require tactile sensing, due in part to a lack of robotic sensors that are delicate enough to interact with food. In this paper we present the design, modeling, and performance of a durometer constructed with soft materials. We performed experiments to investigate the sensor's material selection, repeatability, drift, probing speed, and calibration. We also integrated the sensor into a commercial soft robotic gripper and used it to measure the hardness of an orange. The orange would be damaged by a traditional durometer, but the soft durometer left no visible marks. These results suggest that soft robotic sensors can benefit the food industry and overcome limitations associated with the interaction between robotic systems and fragile objects.**

I. Introduction

Global food supply chains have undergone drastic changes in the last decades as a result of consumer demand for better products at lower prices [1]. In addition to the intrinsic challenges associated with the food market, external factors such as world population growth, volatility in fuel price, and the impacts of climate change have exacerbated the urgency for more flexible and robust processes in the food industry [2] [3].

Producers have resorted more and more to automation. However, this is mostly restricted to picking, placing, packaging and palletizing [4]. Such restriction is imposed by the nature of traditional robotics which is based on the utilization of rigid links, actuators, and sensors. To that end, soft robotics is an appealing framework for developing automated food processors. Compliant robots can adapt to irregular shapes, are gentle enough to handle delicate objects, and can work side-by-side with humans. As an example, the launch of the Flex Picker robot in the late 1990s resulted in improved operational efficiency, and reduction in material movements, vehicle activity as well as in-process stages [4]. Moreover, soft robots have already been applied to strawberry picking [5], tomato harvesting [6], [7], and meat processing [8], [9], [10], and Soft Robotics Inc. has commercialized soft grippers for food handling (among other things). This includes demonstrated pick-and-place operations of steaks, peppers, cupcakes, and many other food items [11]. Manipulation isn't the only function necessary for food processing. One task that human operators often perform and robots must replicate is the sorting of food (fruits for example) based on their hardness. However, measuring hardness presents some interesting challenges. Traditional durometers use standardized probes attached to a spring; The spring applies a constant force, and the displacement of the probe is measured. The more displacement, the harder the material. Unfortunately, these probes would puncture fruit or fish skin since their predefined geometry can induce large stresses on fragile objects. Soft durometers have been implemented using a Gel-sight sensor in conjunction with machine learning [12], or with multi-axis sensor arrays [13], but both of these methods are relatively expensive and bulky.

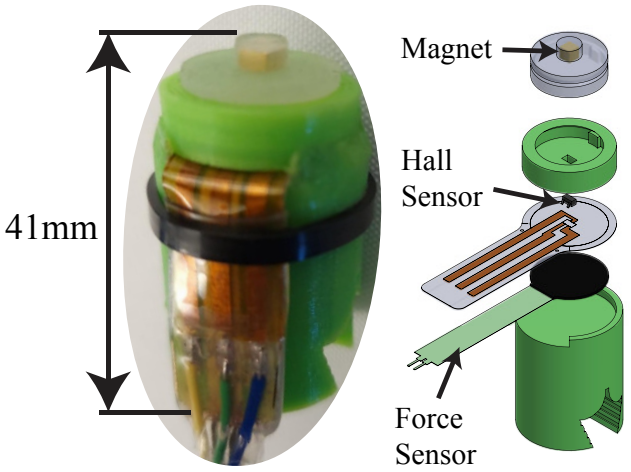

Fig. 1. The soft durometer consists of a magnetic probe, hall sensor, and force sensor encased in a soft body.

Quantifying the stiffness of fragile objects is challenging because it is difficult to construct simple sensing elements that can measure the deformation of these objects without causing permanent damage to them during the loading process. In this paper we present a silicone-based durometer that can be seamlessly integrated into existing soft robots. This sensor combines a force transducer and a hall-effect transducer with a magnet embedded in a soft "probe" to measure compressive deflection of the probe tip (Fig.1). Hall effect sensors have been used in previous soft robots [14], [15],[16],[17],[18],[19], as have rigid embedded elements [20], and the concept of stiffness proprioception as illustrated in [21]. We present the design, fabrication, and calibration of the sensor, characterization of its performance, and demonstration of its use on an orange.

II. Design

The soft durometer includes a force transducer (Interlink Electronics FSR 402) and a hall effect transducer (Diodes Incorporated AH49E) with a 3mm cubic magnet (K&J

[1]This author is affiliated with the Department of Mechanical and Industrial Engineering at Northeastern University, 360, Huntington Ave, Boston, MA, USA. The first author may be reached at oliveira.ma@northeastern.edu

[2]This author is affiliated with the Institute of Experiential Robotics at Northeastern University, 360, Huntington Ave, Boston, MA, USA.

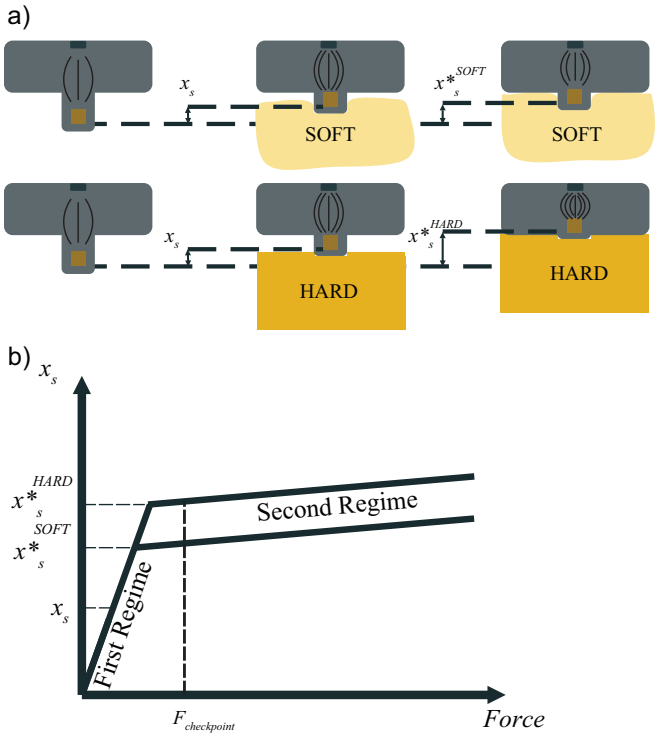

Fig. 2. a) Sensor working principle showing different magnet displacements for targets of different hardnesses. b) Magnet displacement versus force expected behavior for targets of different hardnesses

Magnetics B222G-N52) embedded within a soft probe as shown in Fig. 1. The Hall effect component is vertically aligned with the magnet and is soldered to a flexible copper etched circuit bonded to a polyethylene terephthalate glycol (PETG) laser cut piece and the force transducer. A housing keeps the sensor circuitry and the probe in proper alignment and orientation during loading and unloading conditions. Guaranteeing the proper alignment and normal orientation between the magnet and the hall effect sensor is crucial for accuracy since this transducer detects magnetic field variations perpendicularly aligned with its center.

The operation of the sensor is similar to that of traditional durometers. On contact with the target object, the probe will penetrate the target's surface while simultaneously compressing. Probe compression brings the magnet closer to the Hall effect transducer. As the sensor continues to be pushed into the target, the sensor base will eventually contact the target surface, at which point the contact force will be distributed over the entire sensor face, the force-displacement ratio will change substantially, and the sensing process will complete (Fig. 2a). Qualitatively, the displacement of the magnet relates to the hardness of the target. If the target is much stiffer than the probe, then the magnet will displace substantially. Alternatively, if the target is much softer, then the magnet will not displace.

During the probing process, we typically see two regimes in the relationship between the probe compression (observed through magnet displacement x_s) and force F (Fig. 2b). In the first regime, the probe is the only part of the sensor in contact with the target. Because the probe has a fixed axial stiffness, the force-displacement curve is linear and always has the same slope. The sensor changes regimes when the sensor base contacts the target surface at displacement x_s^*. If the target is much softer than the probe, x_s^* will be much smaller than the probe height h. If the target is much harder, $x_s^* \approx h$. After this transition, the force-displacement curve will have a smaller slope, correlating to the much higher stiffness of the sensor base. We only use x_s^* to determine the target hardness, so we stop sensor engagement at a force $F_{checkpoint}$ shortly after the transition to avoid pushing too hard on the target.

In order to ease the identification of the point at which the change in observed stiffness occurs, it is crucial to design large stiffness ratios into the geometry of the nub and the base of the probe. Because we use a single material for both, we maximized the ratios for the cross-sectional areas of these two sections to achieve this difference.

III. Model

We developed a two-part linearized model to predict the sensor's force-displacement curve and optimize its design for a given range of hardnesses. We considered a system with two coordinates, the magnet displacement x_s and the target deformation x_m. The total displacement $x_t = x_s + x_m$.

In the first regime, the contact between the sensor and the target occurs only over the top of the nub as shown in Fig. 3a. Therefore, only the central portions of the sensor and the target contribute to the overall system's stiffness. We denote the corresponding stiffness of the nub by k_{s1} and the target by k_{m1}, by analyzing the spring systems in Fig. 3a, we obtain the governing equations for the deformation of the magnet, object, and the overall system.

$$F = k_{s1} \cdot x_s = k_{m1} \cdot x_m = \frac{k_{s1} \cdot k_{m1}}{k_{s1} + k_{m1}} x_t \tag{1}$$

The transition point between the two regimes occurs at $x_t = h$, which coincides with the sensor base coming into contact with the target surface. The loading point at which this change takes place is characterized by the transition magnet displacement, x_s^*, as well as the force required for such displacement, F^*.

$$x_s^* = \frac{k_{m1}}{k_{s1} + k_{m1}} h \tag{2}$$

$$F^* = \frac{k_{s1} \cdot k_{m1}}{k_{s1} + k_{m1}} h \tag{3}$$

After the transition, the sensor base is under compression, as well as a larger area of the target, resulting in substantially larger stiffnesses k_{s2} and k_{m2} of the probe and target, respectively.

$$k_{s2}(x_s - x_s^*) = F - F^* \tag{4}$$

Precise values for k_{s2} and k_{m2} are not important, since the hardness is calculated from x_s^*. The important thing is

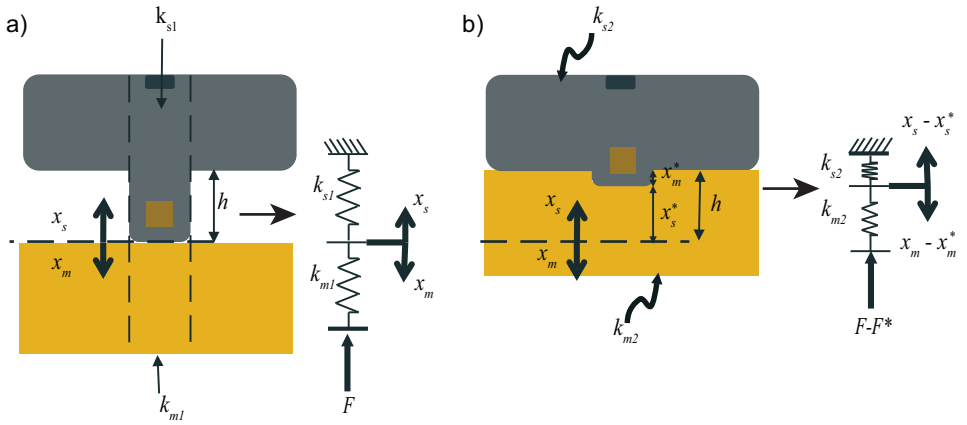

Fig. 3. We modeled the sensor-target interaction as a system of springs. a) First regime showing the contact of an object with the sensor's nub. b) Second regime where object starts making contact with the base of the sensor.

that they are substantially larger than k_{s1} and k_{m1} in the first regime, so that the transition is observable.

Although stiffness and hardness represent different material properties, they are usually tightly correlated. If enough objects of known hardnesses are tested with results recorded for a specific loading point $F_{checkpoint}$ - shortly after the transition point - one can use these results to calibrate the sensor to detect the hardness of untested objects.

IV. Fabrication

Fabrication of the soft probe consisted of a two-step casting process using 3D printed molds (using Formlabs 2) (Fig. 4a). Using a two-part Silicone polymer (Smooth-On, Dragon Skin 10 or Dragon Skin 30) we filled the bottom part of the mold, degassed it in a vacuum pot, inserted the top portion of the mold to form a vertical channel within the silicone, and heated the mold at 60°C for about 1.5 hours. After curing, we inserted the magnet into the vertical channel, covered the straight cut by pouring more silicone up to the surface of the probe's base and placed the system again in the oven at 60°C for about 30 minutes, as shown in Fig. 4b. Finally, we used snips to trim any flashes of silicone produced on the parting lines of the mold.

We 3D printed a housing for the probe using a flexible filament (NinjaFlex, NinjaTek with the Lulzbot Taz 6 printer). The housing was designed to hold the silicone button in place while sitting on top of the hall effect sensor placed underneath it. The circuit that supported the hall effect sensor was made with a flexible sheet of copper-clad polyimide substrate and a solid ink printer (Epson ColorQube 8580) using a previously developed method [23]. To protect the circuit from being torn during the soldering process, we glued it to a laser cut PETG sheet. After soldering the wires and the hall effect sensor to the circuit, the slicone structure was inserted into the holder and all components were aligned. Finally, these components were sandwiched together and held in place by extruding more flexible filament around the circumference of the button holder and the mounting base of the sensor.

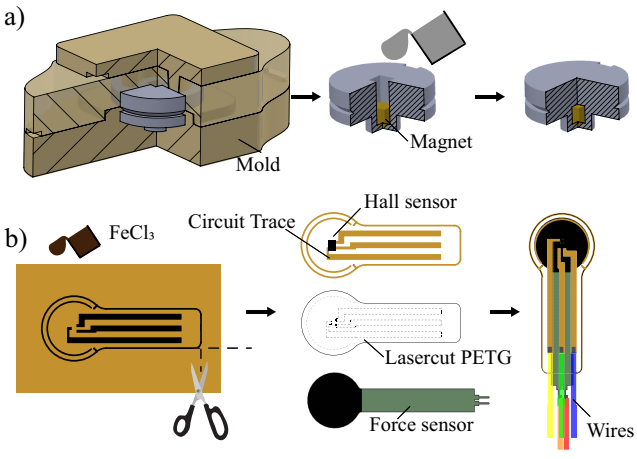

Fig. 4. Fabrication of the sensor probe. a) The sensor probe with the embedded magnet was cast using a three-piece 3D printed mold. b) The force and hall effect transducers circuitry was made by stacking the sensors with a piece of lasercut PETG and flexible circuit obtained through an etching process.

V. Calibration

To calibrate the force and displacement transducers in the durometer, we used a mechanical tester (Mecmesin) equipped with a 250N load cell, connected to a desktop computer for force and displacement data collection. We wired the force transducer in a voltage divider configuration with a $4.7\,\mathrm{k}\Omega$ reference resistor. Both transducers were powered with an input of 5V from a National Instruments USB-6002 data acquisition module (DAQ) which also read their outputs. Sensor data was processed with a moving

	Hardness	100% modulus	Strength
Dragon Skin 10 (DS 10)	10 A	150 kPa	3.3 MPa
Dragon Skin 30 (DS 30)	30 A	590 kPa	3.4 MPa

TABLE I

Sensor material properties[22]

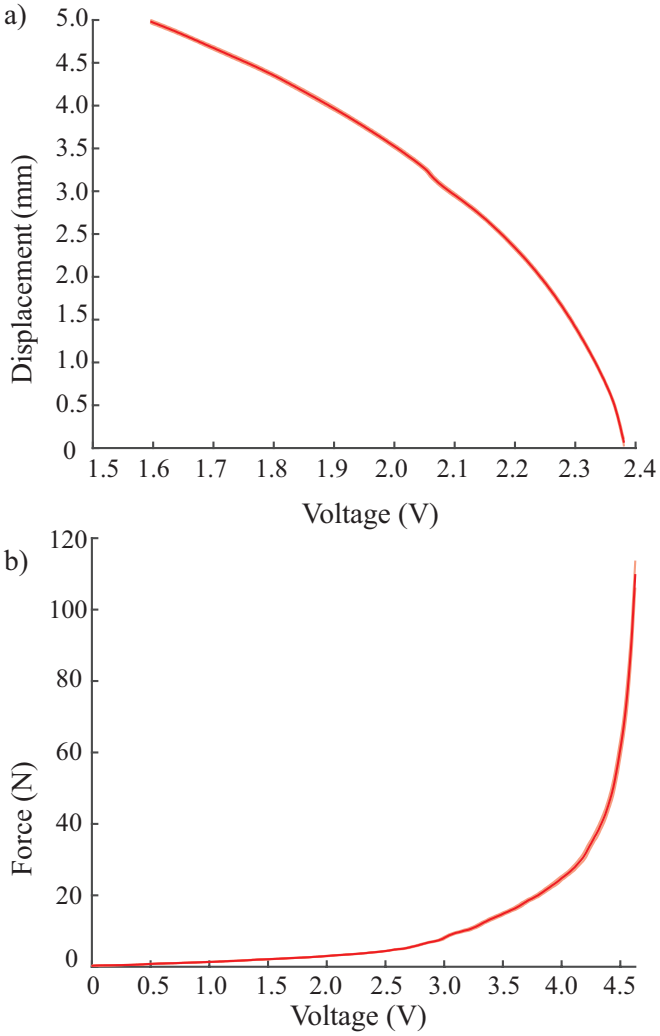

Fig. 5. a) Hall effect transducer calibration curve relating the output voltage with the input displacement. b) Force transducer calibration curve relating the output voltage with the input force. Shaded region indicates standard deviation ($N = 10$).

average filtering data collection script on Labview with an averaging window of 5 samples.

We collected the data by moving the sensor at 32 mm/min for a total displacement of 5 mm while collecting data at 100 samples per second on the mechanical tester as well as the DAQ. A rigid acrylic loadcell probe pushed against the durometer's probe so that loadcell displacement was identical to magnet displacement. We repeated this procedure ten times and observed minimal variance for the transducers (Fig. 5). From these results, we constructed a table relating force and displacement data with the transducers' voltage outputs. A tabular interpolating technique was chosen because of the nonlinear effects associated with the dead zone in the force transducer at lower forces and the material's viscoelasticity.

VI. Experiments

In order to evaluate the performance of the sensor, we ran several tests. In all of them, targets mounted on the moving head of the mechanical tester were loaded against the sensor which was mounted at the stationary base of the tester. We 3D printed fixtures to guarantee that the sensors and the objects were properly aligned throughout the loading process. A LabView routine recorded data upon receiving the triggering signal from the mechanical tester indicating initial contact between the sensor's nub and the object. Force and magnet displacement data were collected at 100 Hz.

A. Repeatability

We built sensors using two different silicones for the soft body: DS10, and DS30. To verify which material would show better performance in terms of sample-to-sample repeatability, we made three sensors of each material, and loaded each sensor three times with a target made out of DS30 (Fig. 6a).

From this figure we observe that sensors made out of DS10 were more repeatable. We believe that the lower viscosity of the uncured silicone in the softer sensor material contributed to a more homogeneous mixture during the fabrication process. Therefore, variations related to the mixing ratio were believed to be more prominent for the harder material. As predicted by the model, the point where the change in stiffness is observed occurs at a larger magnet displacement for this softer sensor. Based on the more repeatable behavior observed for this type of material, we concluded that DS10 would be more appropriate for this durometer and used it for all subsequent experiments.

B. Probing Speed

To observe the effect of probing speed on the sensor, we ran tests at three different speeds. A single sensor made out of DS10 was tested with probing speeds of 28, 32, and 36 mm/min against a target made out of DS30, three times at each speed (Fig.6b).

From these tests we concluded that the sensor responded rapidly enough and showed no time related effects for the probing speeds used.

C. Drift

To evaluate how much drift the sensor would accumulate over time, we tested a single sensor made with DS10 against a target made with DS30 at three different days, one trial a day. The results shown in Fig. 6c indicated no drifting effects on the sensor performance over this time span.

D. Model Validation

We tested the sensor with 12 different targets (EC30, EC50, DS10, MS30, DS30 from Smooth On as well as test block kit from VTSYIQI). The hardnesses of these targets were first measured using a calibrated commercial durometer (Rex DD-3). Each target was then measured with the soft durometer 10 times (Fig. 7). The spread of the curves indicate how targets of increasing hardnesses induced larger magnet displacements in the first regime as expected. Overall, the sensor was clearly able to distinguish between targets of different hardnesses, especially those ranging from 37.82 Shore OO to 68.22 Shore A.

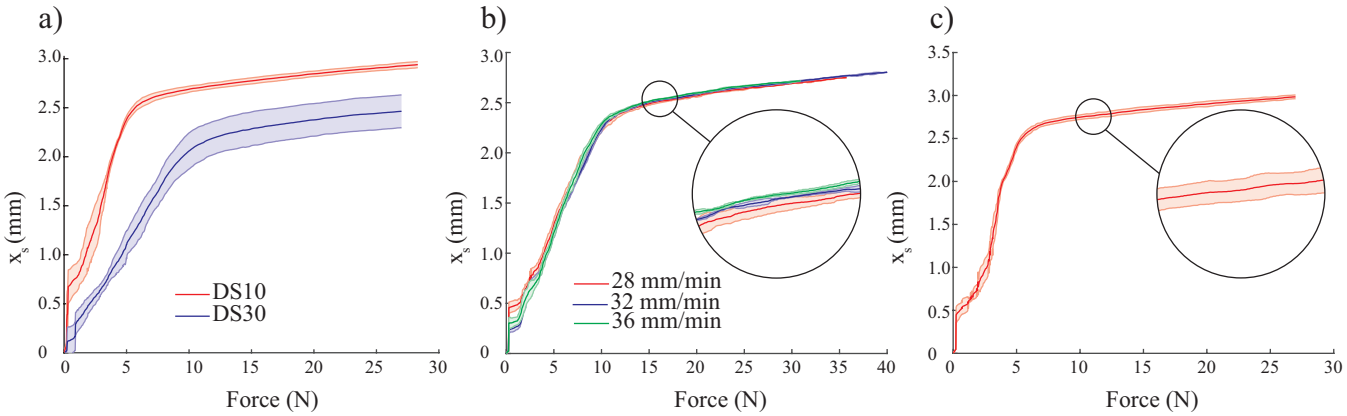

Fig. 6. Experimental relationship between force and probe displacement x_s. a) Results for different sensors made with DS10 (red) and DS30 (blue) bodies. b) Results for a sensor made with DS10 and operated at three different speeds: 28, 32, or 36 mm/min. c) Results for a sensor made with DS10 and tested three days apart. Shaded region indicates standard deviation ($N = 3$).

We observed that for extremely soft targets, we could not apply large forces without damaging the target. Combined with the dead zone of the force sensor, this prevented us from getting more accurate readings. On the higher end of the hardness range tested, the proximity of the curves in the second regime indicated the increased difficulty of the sensor in distinguishing among different targets. This is explained by the fact that the hardness ratio of the target to the sensor's material becomes so large after a certain point that the sensor cannot distinguish as well as it does for softer targets.

In order to compare our analytical model with test results, we superimposed the modeled curves over the test results. We evaluated k_{s1} and k_{s2} for the sensor as well as k_{m1} for each target, using our mechanical tester. The results shown in Fig. 8 for three of the targets tested indicate that the analytical model predicted the test results fairly well. We believe that the discrepancies associated with the results for softer materials were due to the hyperelastic behavior of such materials that become evident at much lower forces. This nonlinear behavior is the reason for a larger error related to the linear approximation made for the stiffness of such materials represented by variable k_{m1}. In addition, the dead-zone and reduced sensitivity associated with the force transducer at lower forces induced a greater impact on the results for these objects.

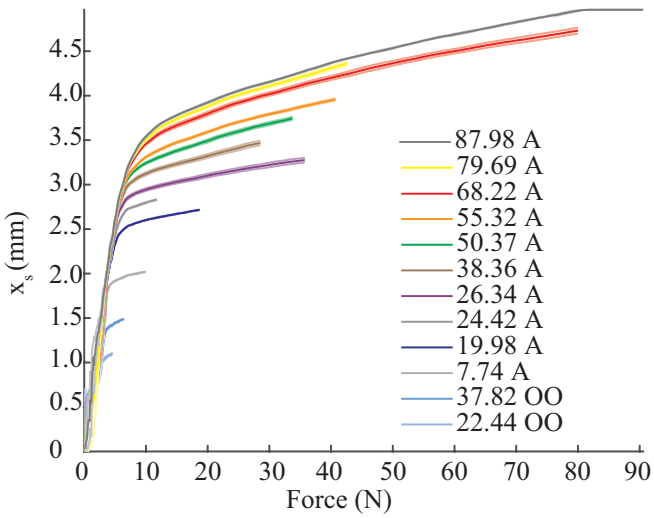

Fig. 7. Experimental results showing the probe displacement x_s as a function of applied force on 12 targets with different hardnesses. Shaded region indicates standard deviation ($N = 10$).

VII. Demonstration

To demonstrate the applicability of our proposed sensor, we developed an automated probing procedure in LabView (Algorithm 1). The procedure was based on the previous selection of force "checkpoints" at which the magnet displacement was checked and linearly interpolated for hardness results based on previous calibration. We utilized the results shown in Fig. 7 along with the hardness values obtained with the commercial durometer to correlate magnet displacement at specific force checkpoints with hardness. For the range of hardness tested, we specify three force checkpoints of 4.5 N, 9.0 N and 18 N, respectively. The lowest force checkpoint was intended for materials harder than 22.44 Shore OO and softer than 7.74 Shore A. The second, for materials harder than 7.74 Shore A and softer than 50.37 Shore A. The third force checkpoint was used for materials harder than 50.37 Shore A and softer than 87.98 Shore A. By implementing different force checkpoints, we avoided pushing targets too hard before receiving a hardness result from the sensor.

We mounted the sensor on the palm of a soft gripper manufactured by Soft Robotics Inc., and tested the sensor on an orange (Fig. 9). For this experiment, the gripper was positioned over the orange and moved down until a hardness reading was obtained. The orange's hardness was also measured with the commercial durometer for the purpose of comparison.

The soft sensor indicated a hardness reading of 25 Shore A with no apparent damage to this fruit. On the other hand, the durometer indicated a hardness of 25x.9 Shore A but left a indent on the orange. Despite the minimal discrepancy

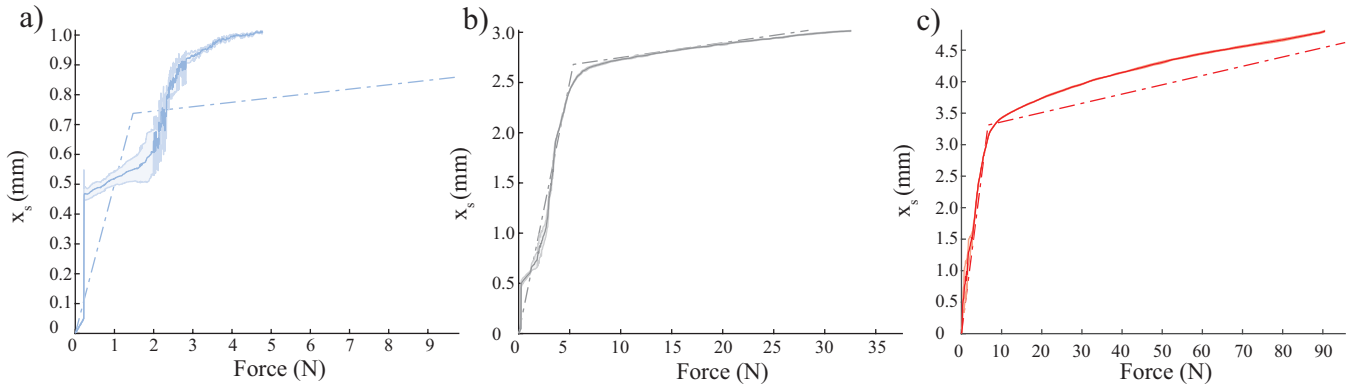

Fig. 8. Experimental results of sensor force and probe displacement x_s (solid lines) along with model predictions (dotted lines). a) 22.44 Shore OO target. b) 24.42 Shore A target. c) 68.22 Shore A target.

between the hardness readings, the safer interaction between the soft sensor and the orange demonstrated the potential applicability of such sensor for food handling purposes.

VIII. Discussion

In this paper we presented the design and performance of a soft durometer intended for food handling. The analytical model indicated that the range of hardnesses can be programmed by the geometry of the sensor probe as well as its material properties. This gives the designer the freedom to optimize the sensor design for applications that demand either a larger range of hardness with less accuracy or a smaller range with more accuracy.

The results suggest that this sensor has good repeatability from sample to sample as well as robustness to drifting effects and different probing speeds. Moreover, the tests indicated that the analytical model proposed predicted relatively well the results. However, some discrepancies due to the nonlinear behavior of the hyperelastic materials tested and the dead zone associated with the force transducers affected the performance of the sensor for softer materials. Further research could investigate how the sensor operates in different orientations relative to both the target surface and gravity.

In order to address these challenges, we believe that other material options should be explored for the sensor probe. In addition, we believe that machine learning techniques, like

Algorithm 1 Hardness Sensing Procedure

$F_1 \leftarrow$ Force checkpoint 1
$d_1^{min} \leftarrow$ Minimum displacement 1
$d_1^{max} \leftarrow$ Maximum displacement 1
$F_2 \leftarrow$ Force checkpoint 2
$d_2^{min} \leftarrow$ Minimum displacement 2
$d_2^{max} \leftarrow$ Maximum displacement 2
$F_3 \leftarrow$ Force checkpoint 3
$d_3^{min} \leftarrow$ Minimum displacement 3
$d_3^{max} \leftarrow$ Maximum displacement 3
$\epsilon \leftarrow$ Acceptable force deviation
while True **do**
  $F \leftarrow$ Force transducer reading
  $d \leftarrow$ Hall Effect transducer reading
  if $F > F_1 - \epsilon$ **and** $F < F_1 + \epsilon$ **then**
    if $d < d_{min}^1$ **then**
      $HARDNESS \leftarrow$ TOO SOFT
    else if $d < d_{max}^1$ **then**
      $HARDNESS \leftarrow$ Interpolated hardness value
    end if
  else if $F > F_2 - \epsilon$ **and** $F < F_2 + \epsilon$ **then**
    if $d > d_{min}^2$ **and** $d < d_{max}^2$ **then**
      $HARDNESS \leftarrow$ Interpolated hardness value
    end if
  else if $F > F_3 - \epsilon$ **and** $F < F_3 + \epsilon$ **then**
    if $d > d_{min}^3$ **and** $d < d_{max}^3$ **then**
      $HARDNESS \leftarrow$ Interpolated hardness value
    else if $d > d_{max}^3$ **then**
      $HARDNESS \leftarrow$ TOO HARD
    end if
  end if
end while

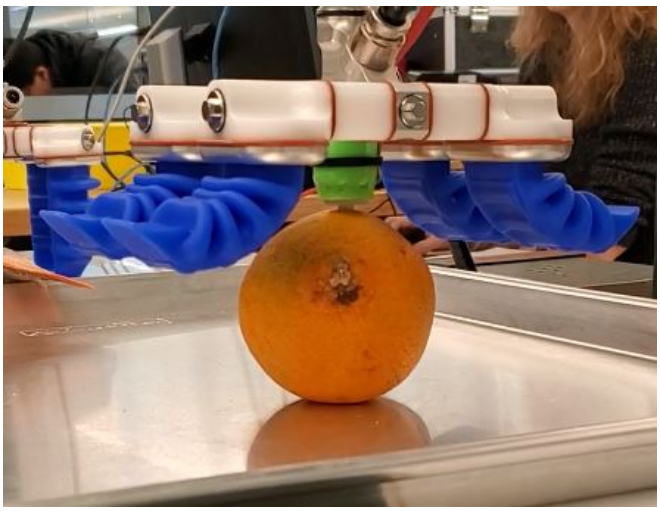

Fig. 9. The soft durometer was mounted on a Soft Robotics Inc. gripper and used to measure the hardness of an orange.

those shown in [24] and [25] could help in the development of accurate algorithms for the detection of hardness without resorting to high probing loads. Nonlinearities associated with hyperelastic materials and surface deformations could be addressed by such techniques. Stiffening mechanisms like those shown in [26], and [27], could leverage the advantages of soft sensors, enabling them to be tuned automatically for different application requirements.

IX. Acknowledgments

This work was sponsored by the Office of the Secretary of Defense and was accomplished under Agreement Number W911NF-17-3-0004. The views and conclusions contained in this document are those of the authors and should not be interpreted as representing the official policies, either expressed or implied, of the Office of the Secretary of Defense or the U.S. Government. The U.S. Government is authorized to reproduce and distribute reprints for Government purposes notwithstanding any copyright notation herein.

References

[1] S. Rahimifard, E. Woolley, D. P. Webb, G. Garcia-Garcia, J. Stone, A. Jellil, P. Gimenez-Escalante, S. Jagtap, and H. Trollman, "Forging new frontiers in sustainable food manufacturing," in *International Conference on Sustainable Design and Manufacturing*. Springer, 2017, pp. 13–24.

[2] E. H. Allison, A. L. Perry, M.-C. Badjeck, W. Neil Adger, K. Brown, D. Conway, A. S. Halls, G. M. Pilling, J. D. Reynolds, N. L. Andrew *et al.*, "Vulnerability of national economies to the impacts of climate change on fisheries," *Fish and fisheries*, vol. 10, no. 2, pp. 173–196, 2009.

[3] J. Melorose, R. Perroy, and S. Careas, "World population prospects," *United Nations*, vol. 1, no. 6042, pp. 587–92, 2015.

[4] J. Iqbal, Z. H. Khan, and A. Khalid, "Prospects of robotics in food industry," *Food Science and Technology*, vol. 37, no. 2, pp. 159–165, 2017.

[5] A. De Preter, J. Anthonis, and J. De Baerdemaeker, "Development of a robot for harvesting strawberries," *IFAC-PapersOnLine*, vol. 51, no. 17, pp. 14–19, 2018.

[6] H. Yaguchi, K. Nagahama, T. Hasegawa, and M. Inaba, "Development of an autonomous tomato harvesting robot with rotational plucking gripper," in *2016 IEEE/RSJ International Conference on Intelligent Robots and Systems (IROS)*. IEEE, 2016, pp. 652–657.

[7] A. Mohamed, J. Shaw-Sutton, B. Green, W. Andrews, E. Rolley-Parnell, Y. Zhou, P. Zhou, X. Mao, M. Fuller, and M. Stoelen, "Soft manipulator robot for selective tomato harvesting," in *Precision agriculture19*. Wageningen Academic Publishers, 2019, pp. 244–255.

[8] M. Stommel, W. Xu, P. Lim, and B. Kadmiry, "Robotic sorting of ovine offal: Discussion of a soft peristaltic approach," *Soft Robotics*, vol. 1, no. 4, pp. 246–254, 2014.

[9] T. B. Jørgensen, B. R. Hansen, M. M. Pedersen, N. Krüger, and N. W. Hansen, "A flexible suction based grasp tool and associated grasp strategies for handling meat," in *Proceedings of the 2018 4th International Conference on Mechatronics and Robotics Engineering*, 2018, pp. 43–47.

[10] H. Rutland, "Novel soft palmar gripper for chicken handling," Master's thesis, Clemson University, Aug 2020.

[11] "Soft Robotics Inc." https://www.softroboticsinc.com, accessed: 2020-09-06.

[12] W. Yuan, C. Zhu, A. Owens, M. A. Srinivasan, and E. H. Adelson, "Shape-independent hardness estimation using deep learning and a gelsight tactile sensor," in *2017 IEEE International Conference on Robotics and Automation (ICRA)*. IEEE, 2017, pp. 951–958.

[13] H. Yussof, M. Ohka, J. Takata, Y. Nasu, and M. Yamano, "Low force control scheme for object hardness distinction in robot manipulation based on tactile sensing," in *2008 IEEE International Conference on Robotics and Automation*. IEEE, 2008, pp. 3443–3448.

[14] M. Luo, E. H. Skorina, W. Tao, F. Chen, S. Ozel, Y. Sun, and C. D. Onal, "Toward modular soft robotics: Proprioceptive curvature sensing and sliding-mode control of soft bidirectional bending modules," *Soft robotics*, vol. 4, no. 2, pp. 117–125, 2017.

[15] S. Ozel, E. H. Skorina, M. Luo, W. Tao, F. Chen, Y. Pan, and C. D. Onal, "A composite soft bending actuation module with integrated curvature sensing," in *2016 IEEE International Conference on Robotics and Automation (ICRA)*. IEEE, 2016, pp. 4963–4968.

[16] E. H. Skorina, M. Luo, W. Tao, F. Chen, J. Fu, and C. D. Onal, "Adapting to flexibility: model reference adaptive control of soft bending actuators," *IEEE Robotics and Automation Letters*, vol. 2, no. 2, pp. 964–970, 2017.

[17] S. Ozel, N. A. Keskin, D. Khea, and C. D. Onal, "A precise embedded curvature sensor module for soft-bodied robots," *Sensors and Actuators A: Physical*, vol. 236, pp. 349–356, 2015.

[18] W. Tao, E. H. Skorina, F. Chen, J. McInnis, M. Luo, and C. D. Onal, "Bioinspired design and fabrication principles of reliable fluidic soft actuation modules," in *2015 IEEE International Conference on Robotics and Biomimetics (ROBIO)*. IEEE, 2015, pp. 2169–2174.

[19] M. Luo, Y. Pan, E. H. Skorina, W. Tao, F. Chen, S. Ozel, and C. D. Onal, "Slithering towards autonomy: a self-contained soft robotic snake platform with integrated curvature sensing," *Bioinspiration & biomimetics*, vol. 10, no. 5, p. 055001, 2015.

[20] D. M. Vogt, Y.-L. Park, and R. J. Wood, "Design and characterization of a soft multi-axis force sensor using embedded microfluidic channels," *IEEE sensors Journal*, vol. 13, no. 10, pp. 4056–4064, 2013.

[21] H. Zhao, K. OBrien, S. Li, and R. F. Shepherd, "Optoelectronically innervated soft prosthetic hand via stretchable optical waveguides," *Science robotics*, vol. 1, no. 1, 2016.

[22] Smooth-On, "Dragon Skin™ Series," http://www.smooth-on.com/tb/files/DRAGON_SKIN_SERIES_TB.pdf, accessed 27 February 2021.

[23] S. M. Felton, M. T. Tolley, B. Shin, C. D. Onal, E. D. Demaine, D. Rus, and R. J. Wood, "Self-folding with shape memory composites," *Soft Matter*, vol. 9, no. 32, pp. 7688–7694, 2013.

[24] T. G. Thuruthel, B. Shih, C. Laschi, and M. T. Tolley, "Soft robot perception using embedded soft sensors and recurrent neural networks," *Science Robotics*, vol. 4, no. 26, 2019.

[25] B. S. Homberg, R. K. Katzschmann, M. R. Dogar, and D. Rus, "Robust proprioceptive grasping with a soft robot hand," *Autonomous Robots*, vol. 43, no. 3, pp. 681–696, 2019.

[26] A. Buso, R. Scharff, E. Doubrovski, J. Wu, C. Wang, and P. Vink, "Soft robotic module for sensing and controlling contact force," in *2020 3rd IEEE International Conference on Soft Robotics (RoboSoft)*. IEEE, 2020, pp. 70–75.

[27] M. Xie, M. Zhu, Z. Yang, S. Okada, and S. Kawamura, "Flexible self-powered multifunctional sensor for stiffness-tunable soft robotic gripper by multimaterial 3d printing," *Nano Energy*, p. 105438, 2020.